INNOVATIVE METHODS FOR WATERWAY INSPECTION: AN APPLICATION TO CANAL-TUNNELS

Emmanuel Moisan[1,2], Philippe Foucher[1], Christophe Heinkelé[1], Pierre Charbonnier[1], Pierre Grussenmeyer[2], Samuel Guillemin[2], Mathieu Koehl[2], Fabrice Daly[3], Stéphane Gastarriet[4], Catherine Larive[5].

ABSTRACT

In this contribution, we propose some innovative methods based on sonar, image and/or laser data acquisition to facilitate the inspection of navigable structures, focusing on canal tunnels. We address the problem of 3D reconstruction of fluvial infrastructures on the basis of three research studies conducted during a doctoral work. In the first study, we evaluated the capabilities of a sonar system by comparing the 3D reconstruction of a lock from sonar and laser data. The second research axis focused on the implementation of reconstruction algorithms of the whole canal tunnel, *i.e.* its above water and under water parts. We relied both on photogrammetric techniques for modelling the above water part of the tunnel and on sonar point clouds for reconstructing the underwater model. Sonar data and images were recorded dynamically and simultaneously from a prototype mounted on a boat. In the absence of GPS signal in the tunnel, photogrammetry is used for computing 3D model of the structure and to estimate he boat trajectory in order to register sonar profiles. The last study aimed at evaluating the experimental 3D model of the tunnel. A reference model of the tunnel has been previously built from static sonar and laser acquisitions. Advanced robust algorithms have been implemented to generate the static model. This evaluation results have shown that the 3D model can locate above water elements with a centimetric accuracy and underwater objects with decimetric accuracy. Finally, we also introduced classification algorithms to automatically detect some defects on tunnels linings. The proposed methods are basic building blocks for the construction of a new generation of inspection methods for waterway infrastructure.

1. INTRODUCTION

Inland navigation is a prime transportation vector, whether for freight or tourism, and represents a more environmentally friendly alternative to road transport. The maintenance of fluvial infrastructures is not only a matter of heritage preservation, but also a commercial necessity and a security issue. Their documentation and periodic inspection is challenging due to the variety and huge number of structures to be considered. For example, Voies Navigables de France (VNF, the French operator of waterways), manages more than 6700 km of waterways (including more than 4000 structures). Filling in the VNF structure database (called BDO) is, for the moment, performed through systematic and exhaustive technical surveys of the structures carried out on site by agents. It is a major effort, may hinder navigation and endanger operators (see Figure 1-left). For this reason, it is necessary to develop highly efficient methods that are minimally invasive to fluvial traffic and require as little human intervention as possible. In this presentation, we focus on a particular type of structures, namely canal tunnels, but the proposed methodologies could concern other waterway structures.

[1] Cerema, Project-team ENDSUM,Strasbourg, France
[2] ICube Laboratory UMR 7357, Photogrammetry and Geomatics Group INSA Strasbourg, France
[3] Cerema, Technical Division Water, Sea and Waterways, Margny-lès-Compiègne, France
[4] VNF, Division Infrastructure, Water and Environment, Béthune, France
[5] CETU, Materials, Structures and Tunnel Durability Department, Bron, France

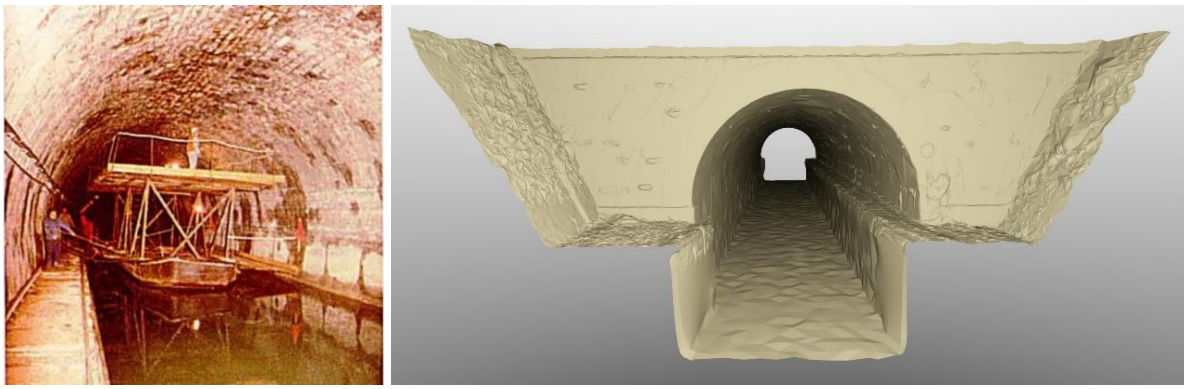

Figure 1: Inspection of the vault of a canal tunnel from a barge (right). The illustration comes from (Fagon Y. 2002). Example of a full 3D model of a canal tunnel (left)

Although there are only a small number of canal tunnels (e.g. in France, 33 tunnels are still in operation, for a total of 42 km of underground waterways), they are key to safe navigation. Located mostly on small gauge canals, they attract heavy touristic traffic. I this paper, we illustrate how up-to-date technologies (3D reconstruction by photogrammetry, high frequency bathymetry and pattern recognition techniques) may be used to design automatic tools for the detection of deterioration on structures and to produce accurate 3D models including both under- and above-water parts of the tunnels, even in the absence of GPS signal. We illustrate an example of such a model in Figure 1-right. In addition to this work on 3D reconstruction, we also explore the use of machine learning algorithms to detect defects automatically on the above-water parts of the tunnels.

With regard to 3D modelling, a doctoral work (Moisan E. 2017) funded by a Cerema scholarship from 2014 to 2017 allowed us to explore the whole-tube 3D imaging of canal tunnels by combining photogrammetry and high-frequency bathymetry sonar surveying. More specifically, three aspects, described in the next sections, were studied:

- evaluation of a recent technology in 3D sonar recording in a lock (Sect. 2)
- development of a 3D reconstruction pipeline based on image and sonar data acquired dynamically from a boat (Sect. 3)
- quantitative evaluation of the 3D model against a reference model of the tunnel, obtained from static laser and sonar acquisitions (Sect.4)

Section 5 is dedicated to pattern recognition algorithms that have been implemented for automatically detecting defects in the infrastructure. Section 6 concludes the paper.

2. 3D SONAR ASSESSMENT IN A LOCK

The objective of this section is to experimentally evaluate the capabilities of a recent multibeam echosounder technology by comparing sonar and laser 3D models built from static acquisitions.

2.1. Experimental setup

The experimental site is lock N°50 of Marne-Rhine canal (Souffleweyersheim, France) whose chamber obeys the Freycinet gauge (Duvergier J. 1879). In December 2015, we took advantage of a complete emptying of the lock for maintenance work to carry out terrestrial laser scanning (TLS) surveys using a *Faro Focus 3D X330* device (Figure 2-left). Once the lock was refilled (see Figure 2-right), static acquisitions were made with the mechanical scanning sonar (MSS) *Blueview BV5000* that consists of the MB1350 multibeam echosounder (MBES) mounted on a rotating mechanism.

Figure 2: View of the empty lock during the TLS surveying (left) and the lock after refilling during the MSS surveying (right)

It may be noticed that for the TLS survey, six scanner acquisitions were made from the bottom of the empty lock (Figure 3-a) and eight stations from the top of the lock. Spherical targets were placed around the lock chamber in order to facilitate the registration of scans. For the sonar, two acquisition configurations took place: three acquisitions were made with the sensor on a tripod at the bottom of the lock (Figure 3-b). In the other configuration, the device was immersed, upside down from the surface (Figure 3-c). To do this, the device was attached to a metal mast, which was fixed to a ladder placed transversely on the lock. In this configuration, a tacheometric prism was attached to the device mast. The sonar positions can thus be carefully surveyed with a total station. With this suspended configuration, the acquisitions were made every 5 meters, providing 9 point clouds. For each station, the sonar head performed three 360° rotations around its vertical axis, with a *15*°, *-15*° and *-45*° tilt angle, successively.

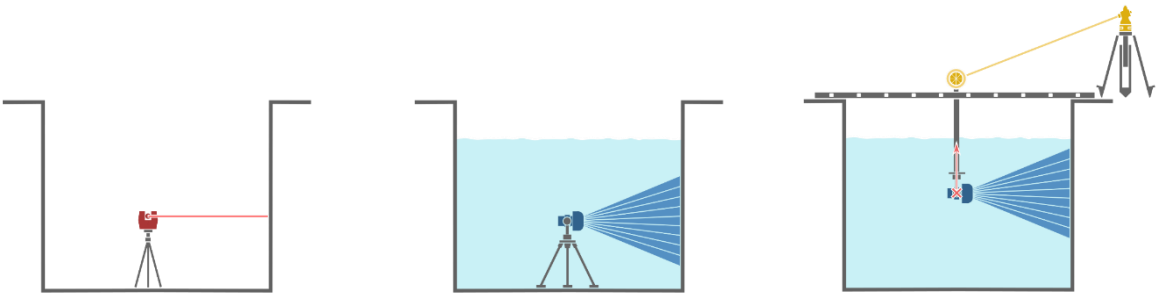

Figure 3: Terrestrial laser scanning (the device is in red) in the empty lock (left). Surveys of sonar point clouds in the filled lock. The device (in blue) is placed on a tripod at the bottom of water (middle) or suspended on a ladder and immersed upside down (right). The tacheometric prism (attached to the mast) and the total station (on the dock) are shown in yellow

The alignment of TLS point clouds was performed using *FaroScene* software with a sub-centimetric accuracy. The resulting model is illustrated on Figure 4-top. For the reconstruction of the 3D sonar model, there are no spherical targets in the water and the horizontal orientations of the scans are unknown. An original method must therefore be implemented to consolidate the model. This process includes a first step of translation and levelling through conventional topographic methods thanks to the prism positions and a second step in which point clouds are oriented horizontally using an *ad-hoc*

methodology. The entire registration process is described in (Moisan E. 2016). The resulting subaquatic model is shown in Figure 4-bottom.

Figure 4: Complete model of the lock from terrestrial laser scanning (top) and mechanical sonar scanning (bottom). Colours represent the scans of the 9 sonar static acquisitions

2.2. Results

The analysis of the sonar model focuses on three aspects. First, this experiment made it possible to assess the imperfections observed on the sonar point clouds. The second analysis is a quantitative evaluation of the 3D sonar model compared to the model obtained from the laser point cloud, considered as a reference. The final analysis aims at qualitatively assessing the possibilities of visualization and identification of details.

- **Artefacts**

Figure 5 shows the grainy aspect of the sonar model compared to the TLS one. In particular, we observe that the granularity of the MMS data increases with the distance from the acquisition station. Noise, inherent in the sonar measurements, explains some of these inaccuracies. It should be noted that the size of the sonar footprint increases with the distance from the sensor and the angle of incidence of the beam. Hence, we observe that the MSS model appears more granular in these unfavourable situations, i.e. long distance and at grazing incidence angles. This phenomenon is all the stronger in narrow environments such as tunnels or locks. This experiment also highlighted various artefacts in the sonar data. The first disturbance is due to the reflection of the signal on the water surface, as shown in Figure 6-left. This artefact can be easily filtered out if the water level is known. In our experiments, this level was measured with a tacheometer. We also observe acoustic anomalies that produce ghost objects. Artefacts related to backscattering of the sonar signal on a surface can occur and lead to the appearance of systematic shapes (Figure 6-left). For these two types of disturbances, manual filtering of outliers was performed before cloud consolidation. Finally, material dysfunctions can generate acquisition artefacts or the lack of acquisitions, as illustrated in Figure 6-right.

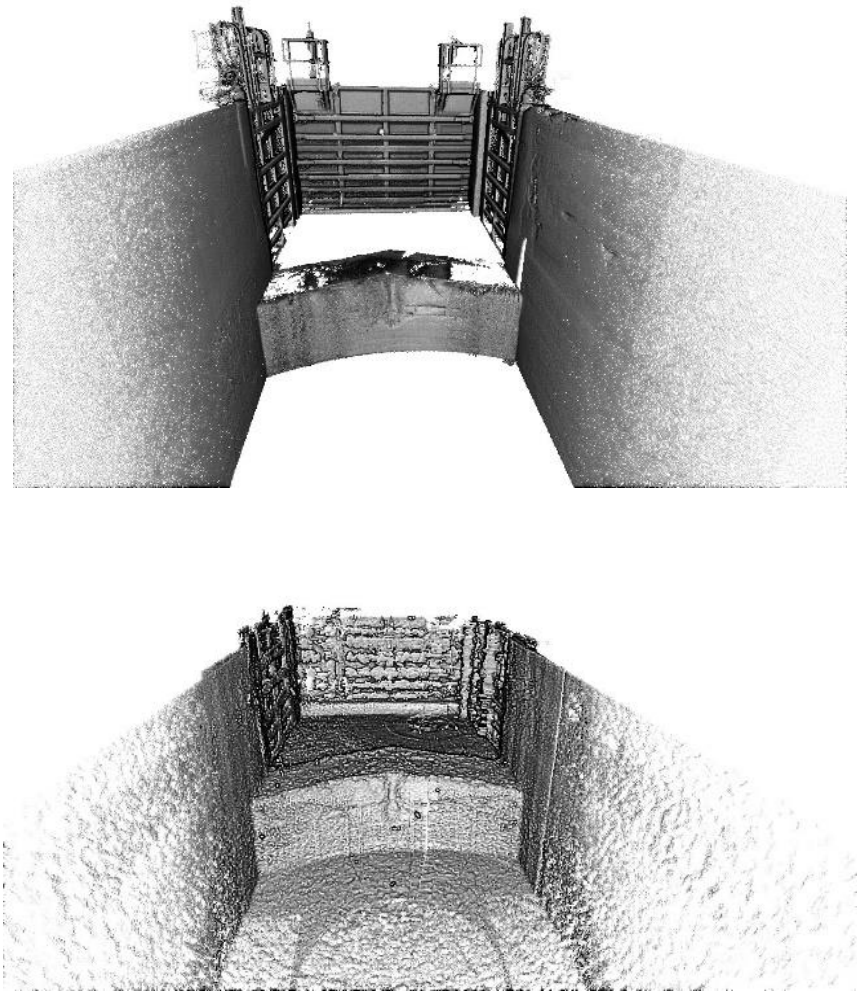

Figure 5: Laser (top) and sonar (bottom) models of the upstream lock gate

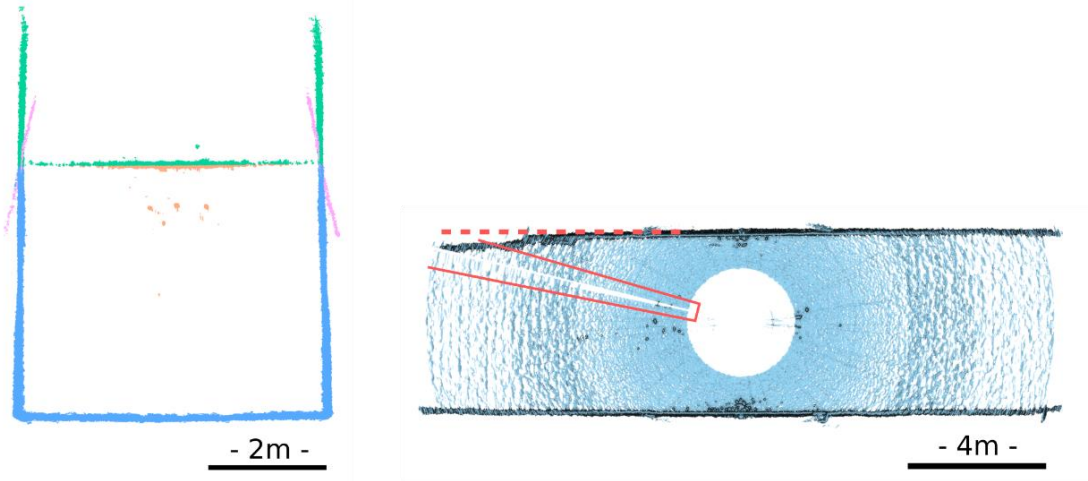

Figure 6: Examples of disturbances in sonar data: artefacts due to surface reflections (in green, left image), acoustic anomalies in the water column (in orange, left image), acoustic phenomena due to signal backscattering (in purple, left image). Acquisition anomaly (dashed line, right image) and lack of sonar measurements (red box, right image)

- **Quantitative assessment**

By working in the same coordinate system, we were able to compare the 2 models (MSS and TLS) by calculating the distances between both reconstructions. Note that the sonar model is a point cloud and the laser model is a mesh. It may also be noticed that we have restricted this quantitative analysis to the lock walls, considered separately. Results are gathered in the table 1.

Table 1: Distance analysis between the laser mesh cloud and the SONAR point cloud. By convention, distances are positive when the sonar points are inside the laser model

	Left wall	Right wall	Total
Mean	2.0 cm	1.8 cm	0.1 cm
Standard deviation	2.3 cm	2.4 cm	3.1 cm
Max	10.7 cm	10.3 cm	10.7 cm
Min	-6.5 cm	-9.8 cm	-9.8 cm

The differences between the sonar and laser models are in the range (-9.8, 10.7) cm. The mean (considering both walls simultaneously) of the distances is 0.1cm and the standard deviation is 3.1cm. However, by analyzing the means of the deviations for each wall, we observe a bias of about 2 cm. This bias represents a slight translation between the sonar and laser models transversely to the lock axis.

- **Visualization of details**

In this study, we analyse the sonar capabilities to distinguish details of the lock structure. We focus on two areas of the lock. In the first one, a rubble stone (approximate dimensions: 60x20x10 cm) was missing (Figure 7-a) and masonry joints are damaged (these cracks are about 4 cm wide and 4 cm deep). In the second area, we observe a cavity (approximate size: 50x100x15 cm) due to a spall (Figure 7-c). In the Figure 7-b,d, we can see that defects larger than 5 cm, such as stone defects or cavities, can be observed on the sonar model. Smaller details, such as damaged masonry joints are harder to detect. This experimental analysis highlighted the minimum size of defects that can be seen on a sonar model.

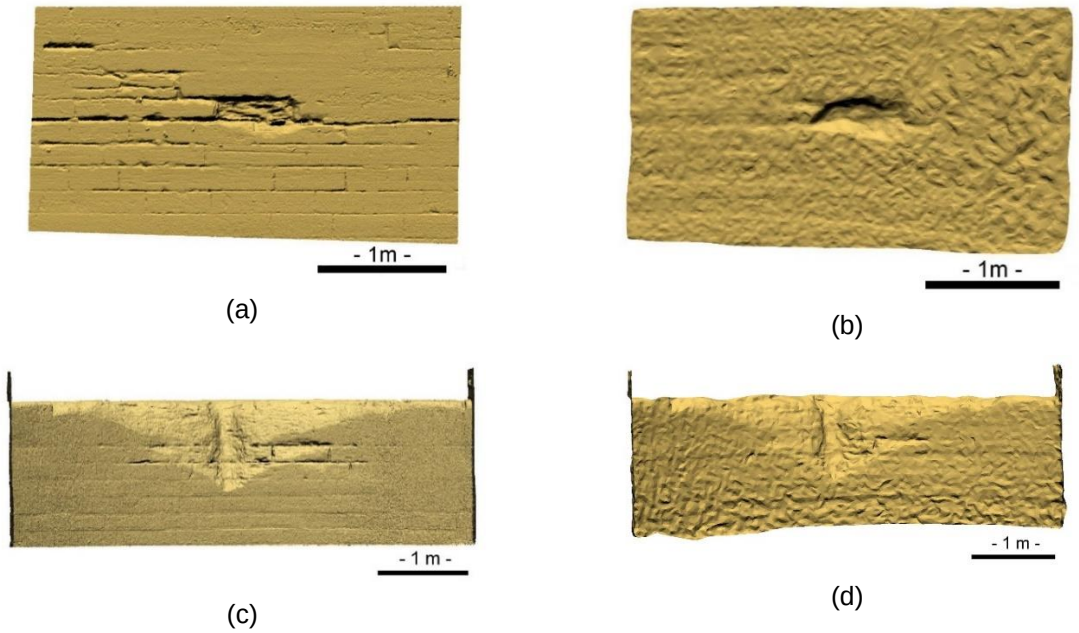

Figure 7: Details on the walls of the lock. Views of a lack of rubble stone on laser (a) and sonar (b) models. Views of cavities on laser (c) and sonar (d) models

3. FULL 3D MODEL OF A CANAL TUNNEL

The full 3D model of the canal-tunnel was built from images for the out-of-water part and bathymetric data for the underwater part. Images and sonar data were recorded simultaneously, in a dynamic fashion, from an acquisition prototype. The above-water part of the tunnel was reconstructed using photogrammetric techniques. However, given the high number of images, it was necessary to organize data to reduce computation times. For the underwater part, we used the trajectory of the boat for registering 3D sonar profiles. In traditional bathymetry, this trajectory is generally determined thanks to GPS tracking, possibly coupled to an inertial unit. In the case of tunnels, GPS signals are unavailable, and an inertial unit, used alone, may drift rather quickly. We therefore proposed to take advantage of photogrammetric methods to estimate the camera pose at each acquisition and thus, to retrieve the trajectory of the boat. Thanks to a preliminary determination of the system geometry, i.e. the relative positions of the sensors (cameras and sonar), we could consolidate the sonar profiles and compute the underwater model. The method is summarized in Figure 8.

3.1. Acquisition system

Since 2009, a French partnership composed of VNF, The Centre d'Études des Tunnels (CETU) and the CETE de l'Est (now the Cerema) in collaboration with the Photogrammetry and Geomatics Group of INSA has developed a visual inspection system dedicated to canal tunnels from acquisitions of image sequences. A modular prototype with lightings and cameras, mounted on a barge, has been devised for recording images of the vaults and sidewalls of the canal tunnel (see Figure 9). It may be noticed that the cameras can be oriented at several angles in order to visualize different areas of the vault. The imaging system consists of six 1920 x 1080-pixel resolution cameras. The image acquisition was triggered at a frequency of 5 Hz and synchronously for all cameras. It may be noticed that among these 6 cameras, there were two pairs of stereovision cameras: one pair to visualize the sidewall and the other for the vault. This second pair can be oriented at different angles to acquire images of all areas of the vault. The two remaining cameras have oblique sights to facilitate photogrammetric reconstruction.

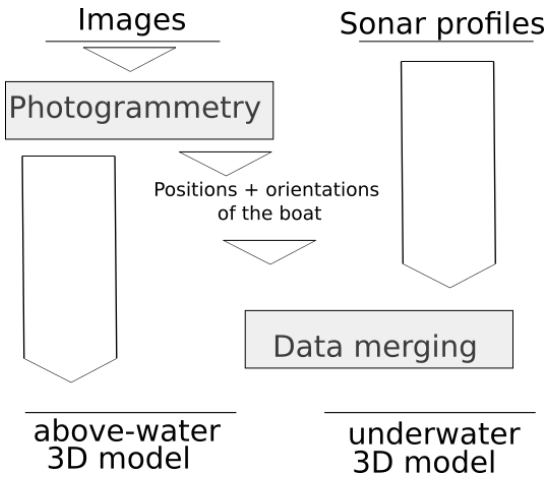

Figure 8: Methodogy for 3D reconstruction of a canal tunnel

The sonar device (MB1350) was attached to the front of the boat thanks to a removable pole. The sonar is oriented perpendicular to the canal axis. The device could be fixed to the pole with different acquisition angles. The aperture angle of the swath was 45° and sonar profiles were recorded at a frequency of 40Hz.

As the boat speed was about 1 $m.s^{-1}$, the inter-distance between two successive images was about 20 cm and, between two sonar profiles, about 2.5 cm. Moreover, a set of points and targets, previously implemented inside and outside the tunnel, has been surveyed for georeferencing the model (see Figure 10).

Figure 9: Our acquisition prototype mounted on a barge at the entrance of the tunnel (left) and inside the tunnel (right)

The tunnel where the experiments took place is located in Niderviller, on the Marne-Rhine canal in France. It is straight, 475 m long, covered in masonry and equipped with a pedestrian path on the ledge. We refer the reader to (Charbonnier P. 2014) for further details on this tunnel. For the experiment, three back and forth passages inside the tunnel were necessary to record data for the whole vault and the sub-aquatic part of the tunnel. Thus, a total of 3 sonar angles (11,25°, 45°, 90°) and 2 orientations of a stereovision pair had been planned to collect data for the entire tunnel (see Figure 11). Finally, for all passages, 90,000 images and 120,000 sonar profiles were collected.

Figure 10: Examples of targets viewed in the images. Catadioptric plate (left) and lasergrammetric target (right)

3.2. System calibration

Prior to the acquisitions, the system must be calibrated to allow the trajectory of the sonar to be deduced from that of the rigid block formed by the cameras. First, the focal length, the optical centre coordinates

and the coefficients for distortion correction of the cameras were determined (intrinsic calibration) (Zhang Z. 1999). Stereovision rigs were also calibrated in order to measure in 3D (Tsai R.Y. 1987).

The geometric calibration, second step of the process, consists in determining the physical offsets between sensors (or lever-arm). To compute these distances, the whole system was scanned using TLS device, as shown on Figure 12. To carefully determine the positions of the device acquisition centers in the laser model, the CAD (*Computer-Aided-Design*) models of the sensors, given by the manufacturer, were matched with the point cloud. Note that the sonar system was surveyed onshore. the model of the system (in red in Figure 12) and that of the sonar (in blue in Figure 12) were aligned from the geometry of the emerged part of the attachment pole. The offsets were then directly computed on the TLS model. Based on these relative positions, the sonar trajectory could then be estimated from the camera poses.

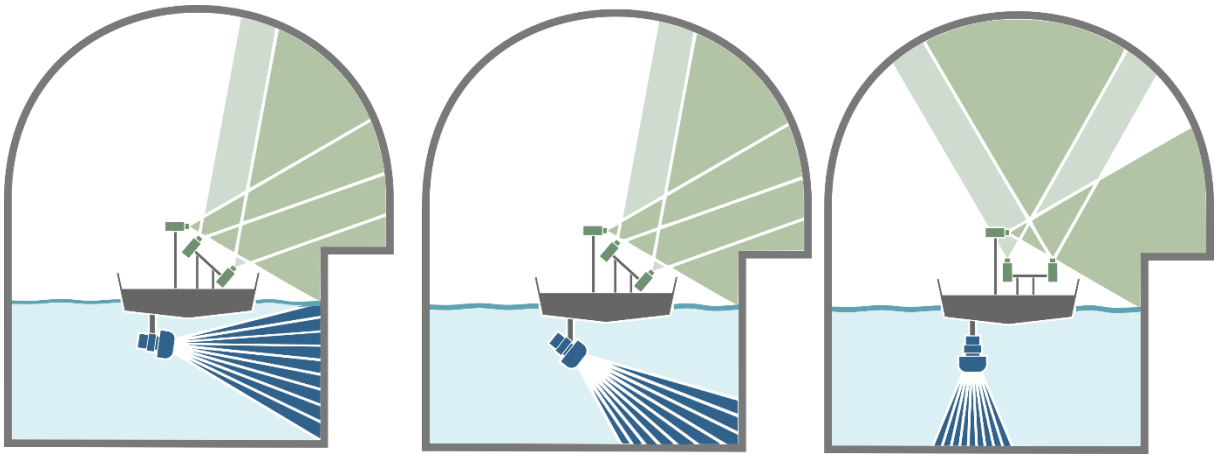

Figure 11: Sensor configurations with 3 sonar angles and 2 stereo rig angles

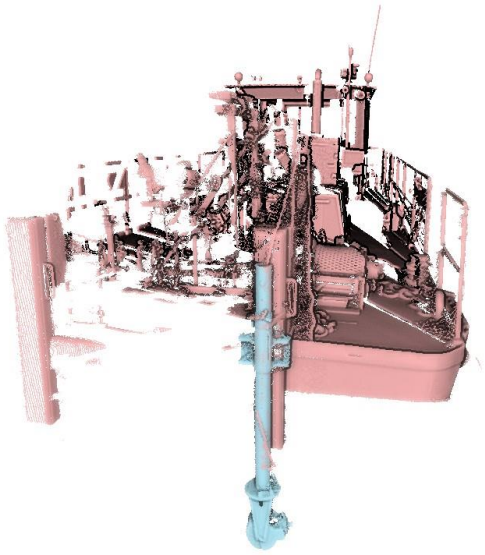

Figure 12: Whole system scanning for estimating the geometric calibration (lever-arm). The sonar device and its pole (in blue) are actually scanned onshore

3.3. 3D reconstruction

Considering the large amounts of data resulting from acquisitions, photogrammetry cannot be used directly for modelling the tunnel vault. It is necessary to implement a suitable methodology, which can be defined in two stages. First, we exploit the depth-disparity relationship of a calibrated stereovision system (Szeliski R. 2010) for pre-locating images. The difference, in pixels, between the position in the image of two points in two views of the same scene (disparity) is inversely proportional to the depth of the point in the scene. The proportionality coefficient depends on the difference, in meters, of the position between the two shots (stereo base). More specifically, applied to the stereo rig facing the sidewall, we can use this relationship to estimate the relative motion between two successive image acquisition positions, as detailed in (Albert J.L. 2013). Note that, as with any other relative location methods, positioning tends to drift due to error accumulations. We tackled this difficulty by using georeferenced points to readjust positions (Figure 10).

The second step consists in reconstructing the model itself. For computation reasons, it is impossible to process all the images at once to generate the tunnel model in a single piece. Therefore, we cut the tunnel into small sections (see Figure 13) that we call tiles. These tiles are modelled one by one and then aligned with each other. Typically, the length of a tile is 2m. Thanks to the pre-localization tool presented above, selecting and ordering the images of a tile is simplified.

Figure 13: Tile registration using Photoscan® software

Two softwares, MicMac (Rupnik E. 2017) and Photoscan[6], were tested for the photogrammetric computation of tunnel section models. Both computer tools provided similar results. A 2 m-sub-model is shown in Figure 13.

[6] http://www.agisoft.com/

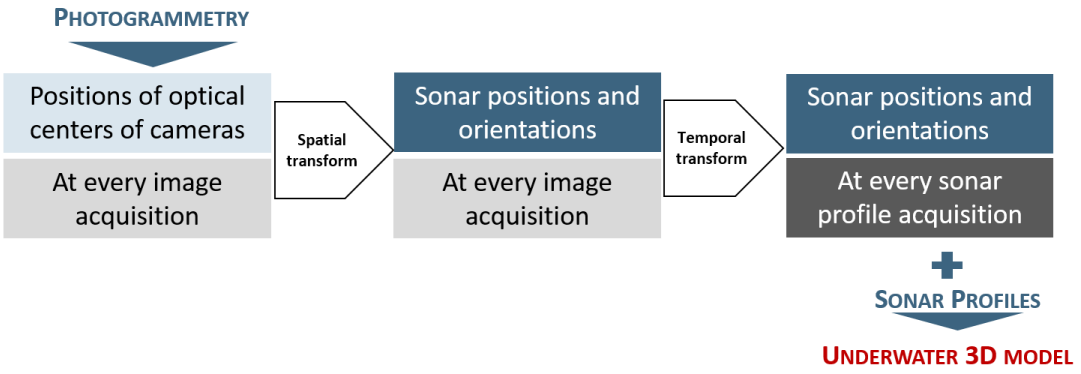

Figure 14: Sonar profiles referencement

Modelling the underwater part amounts to aligning the point profiles recorded by the multibeam echosounder. As shown in Figure 14, the reconstruction method of underwater model needs a spatial and a temporal transformation. First, the spatial transform aims at computing the absolute position and orientation of the sonar at each image acquisition. We aligned camera positions in the relative calibration system to their absolute locations, given by photogrammetry. We used the Procrustres method (Golub G.H. 2012) to compute both translation and rotation matrices. In the temporal-transform step, we synchronized sonar and images acquisitions by interpolations. Linear interpolations were applied to determine the sonar positions and spline interpolations were used to compute sonar orientations at every sonar profile acquisition. A “full-tube” 3D model of the first 30 meters of the tunnel was obtained in this way. The result illustrated in Figure 15, has been generated using Photoscan software.

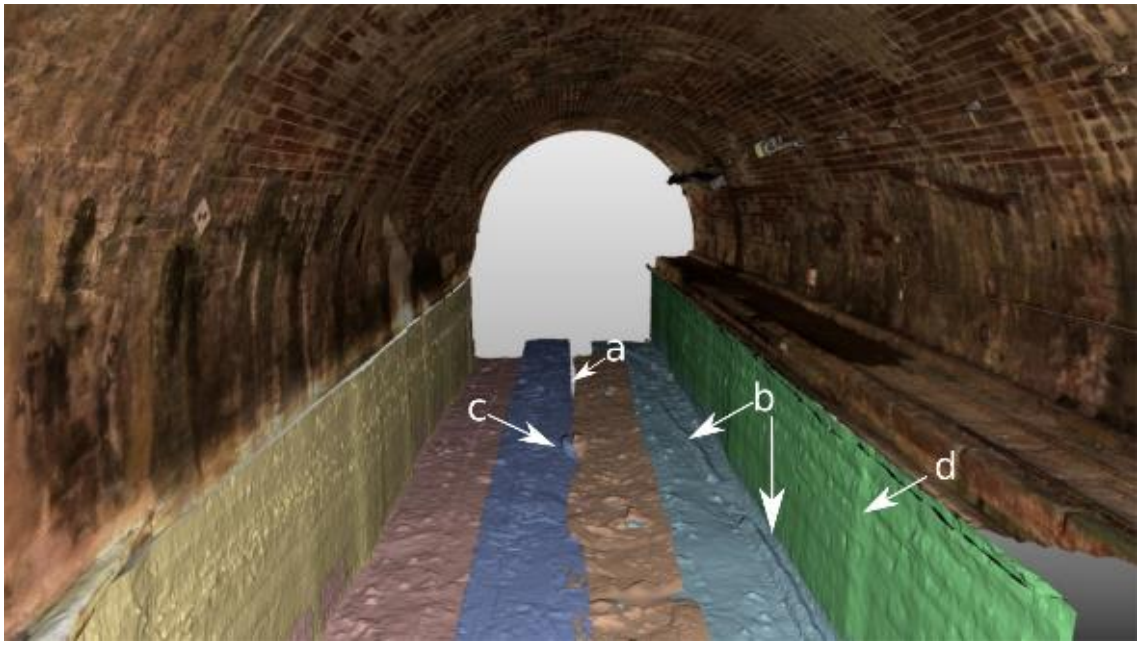

Figure 15: 3D model of the entrance of Niderviller tunnel. Colours represent the 6 different passes in the tunnel

Qualitative analysis of the resulting model shows that the juxtaposition of the photogrammetric and sonar models appears to be fairly consistent overall. The acquisitions from the different sonar passages also complement each other correctly. However, some gaps can be seen between passages due to the absence of measurements (see Figure 15, indication *a*). Some objects can also be seen on the bottom of the water, such as slide-rails (made of tropical wood, denser than water) that fell off the wall (see

Figure 15, indication *b*) and a cylindrical object, possibly a vehicle tyre (see Figure 15, indication *c*). Finally, we notice that the walls do not appear completely straight, when in fact they are. These discontinuities, illustrated by the indication *d* in Figure 15, are perhaps linked to the way the tiles are agglomerated. This discontinuity issue can be reduced by taking better account of the continuity of the trajectories between the tiles. An in-depth qualitative analysis is described in (Moisan E. 2017).

4. QUANTITATIVE EVALUATION OF 3D MODEL

4.1. Reference model

To quantitatively assess the accuracy of the 3D model, a reference model was built from static acquisitions. In practice, the entrances of the canal tunnel were surveyed by combining laser and sonar technologies (Figure 16-left).

A terrestrial laser scanner *(Faro Focus 3D X330* device) was used to scan the above-water part of the tunnel entrances from two stations (per entrance), located on either side of the canal. Spherical targets, visible on Figure 16-right, were placed around the environment to register TLS point clouds. The coordinates of the centres of the spheres were surveyed by conventional topography. Moreover, a set of reference points implemented on site is used to georeference model in the French reference coordinate system. The mechanical scanning sonar (BV500) recorded underwater data simultaneously with TLS acquisitions. At each entrance, two separate 10 m MSS static acquisitions were performed, one inside the tunnel and the other outside. MSS, mounted on a tripod, was immersed from a boat and stabilized at the bottom of the canal. Two wooden ladders, with known geometry, were partially immersed in the canal (Figure 16-right). They were scanned by both TLS and MSS devices.

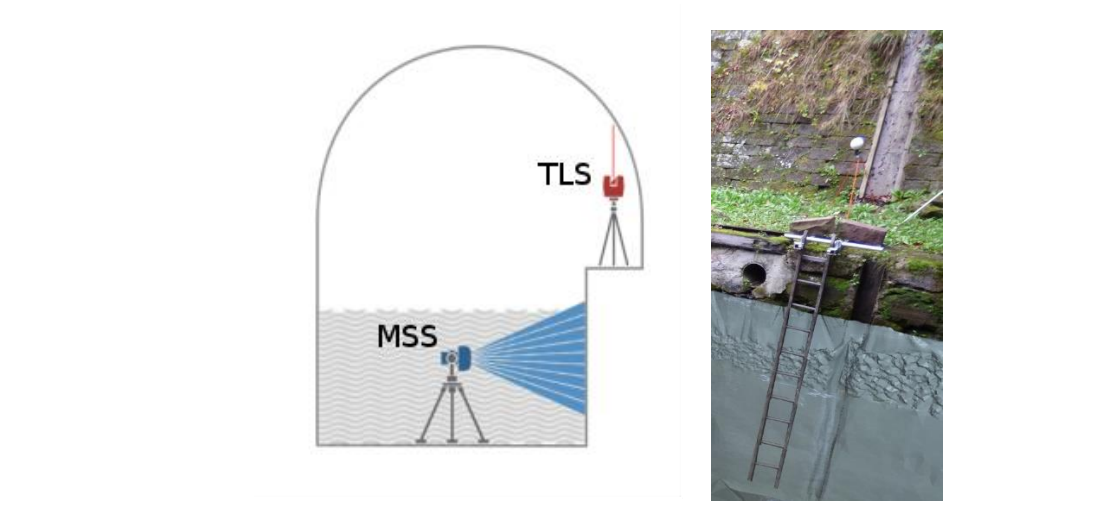

Figure 16: Experimental setup for laser and sonar scanning. Schematic representation of TLS and MSS stations (left). Ladder (synthetic representation for the underwater part) and sphere (in the background) positioning (right)

To generate the complete tunnel model, a possible approach consists in aligning sonar and laser models. However, this method would require an overlap between the two point clouds, which is not the case due to the different natures of the laser and sonar acquisitions. Hence, a methodology had to be implemented to reconstruct the model. In summary, the proposed method is based on geometric elements of the infrastructure (orientation of wall planes or ridges), known objects (ladders) and features extracted from the silhouette of waterline. This information has been extracted, using advanced robust algorithms and measured in underwater and above-water models in order to align them. We refer the reader to (Moisan E. 2015) for detailed explanations about the 3D reconstruction method of the

reference model. Figure 17 shows a meshed view of the resulting georeferenced model of the tunnel entrance.

Figure 17: Reference model of the west entrance of the canal tunnel. The dark disk in the middle of the canal indicates the location of the MSS station

4.2. Comparison between dynamic and reference models

We focalised the evaluation of the 3D model on the west entrance of the tunnel. The distances of the dynamic model (point cloud) to the reference model (mesh) are computed using Cloudcompare[7] software. The quantitative results show a significant difference between accuracies of photogrammetric and sonar models. The photogrammetric model (with Photoscan software) has an accuracy of 1.1 cm with a standard deviation of 1.1 cm. The approach that we have implemented to reconstruct the vault and the sidewalls of the tunnel seems relevant. Figure 18 highlights that the distance distribution to the reference model is not homogeneous. We observe stripes with large distances, transversely to the tunnel axis. It may be explained by an error in the alignment of some sub-models. Small deviations are often located in areas close to reference points.

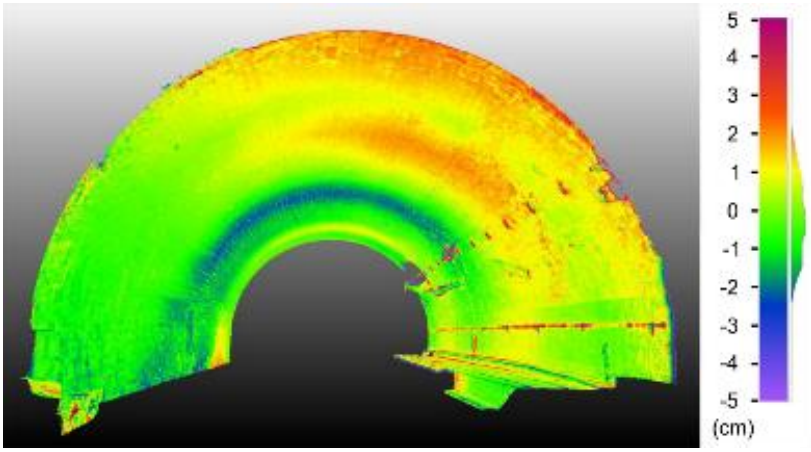

Figure 18: Visualization of the distances between the photogrammetric model and the reference model

[7] http://cloudcompare.org/

The evaluation of subaquatic models (the 6 passages are considered separately) reveals an accuracy in the range (5.7, 14.7) cm and a standard deviation in the range (1.9, 7.8) cm. These differences in accuracy with photogrammetric evaluation have several explanations: errors in the photogrammetric model, errors in the estimation of the system calibration or inaccuracies of MSS point clouds.

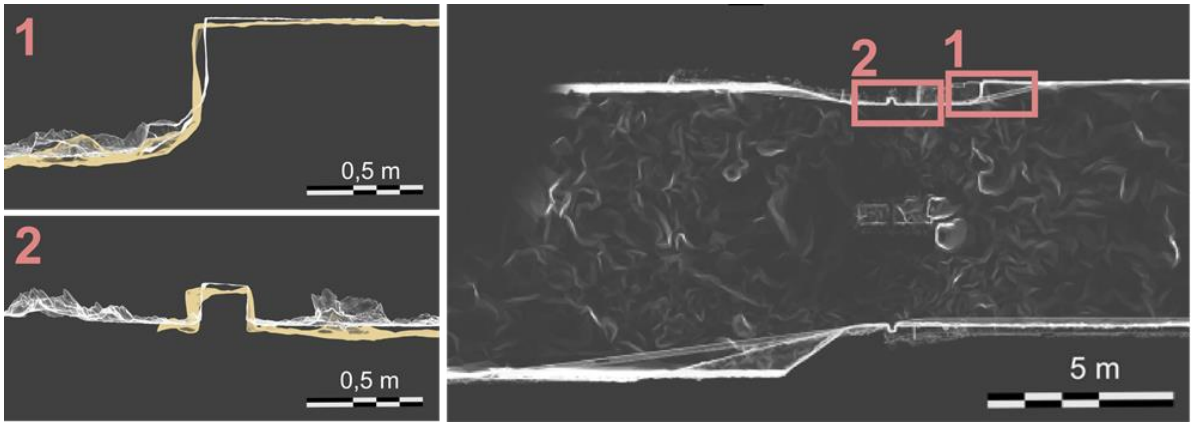

Figure 19: Overlay (with transparency) views of sonar (in orange) and laser (in white) models (left). Top views of the model (right) with the two areas of interest

Note that, by chance, a part of the sidewall was above water for static acquisitions (recorded by TLS) and under water for dynamic experimentation (scanned by sonar). We took advantage of this difference (10 cm) of water height in the canal to visualize some deviations (Figure 19). It may be seen that the details appear in the model at a position close to the reference points (Figure 10). The differences are about a few centimetres, which is consistent with our quantitative evaluation.

5. DEFECT DETECTION

Beyond 3D modelling infrastructures, an important point for tunnel inspection is the automatic detection in tunnel images. It is a challenging issue, due to the variability of situations in terms of tunnels and defects. Here too, advanced technologies and more specifically, machine learning *techniques*, are capable of providing high-performance tools. In this section, we explore a classification algorithm to detect and localise cracks, water leaks, exposed concrete reinforcements and damaged masonry joints in tunnel linings.

5.1. Classification method

The method we want to devise aims at detecting defects that are located in small parts of the images of the tunnel (Figure 20). It relies on a classification algorithm (or, in short, a *classifier*) whose role is to assign each image sample into a previously defined category, e.g. “defective” or “healthy” to characterize a surface state, “concrete”, “masonry” or “rock” to categorize a lining. In practice, images are not considered directly. Actually, different representations of them, called features, are used at the classifier input. The choice of the features depends on the observation of representative samples of the classes and on the knowledge of the problem to solve. In our work, we used features that relate to pixel values and their local relationships (Dalal N. 2005), contours (Xiao Y. 2014), or texture (Haralick R. 1973) gathered into feature vectors of about 3800 numbers.

In a first phase (supervised learning), a number of samples of each category are extracted from images. The corresponding feature vectors are presented to the classifier. Each vector having previously been labelled, the algorithm optimizes its internal representation to ensure the best possible correspondence

between its outputs and the expected labels. In the second phase (classification), the analyzed image is scanned using a sliding window. Each extract is transformed into a vector of characteristics, which is presented to the classifier who then assigns it a label. Of course, different images are used for training and for classification.

In this preliminary work, we relied on the Random Forest algorithm (Breiman L. 2001) to perform the classification task. More details about our implementation of the method may be found in (Foucher P. 2016).

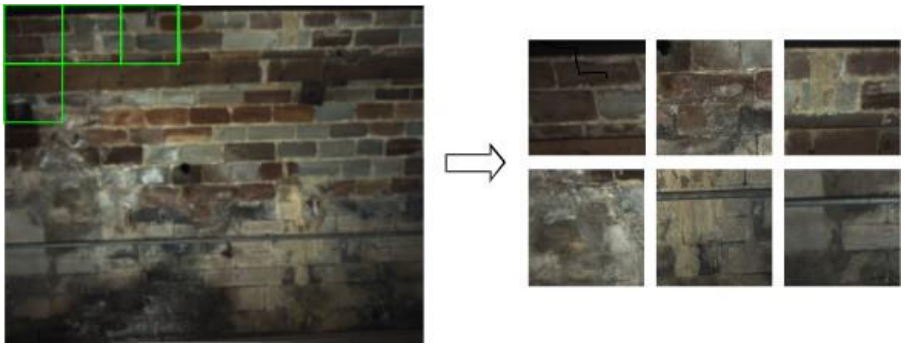

Figure 20: Extraction of samples (green rectangles) over the whole tunnel image. Every sample is classified into a category.

5.2. Results

We evaluated the classification method through two experiments. For each experiment, we selected a set of images to perform the learning process and evaluation. Approximately 500 samples per class were extracted from the images. The images that were not selected for the learning, were used to visualize and evaluate the performances of the algorithm on full-size images along the tunnel.

In the first experiment, we are interested in detecting moisture or more generally water leaks on images of a masonry tunnel. Each sample can be classified into category “water leaks” or “normal lining”. The sample evaluation provides a true positive rate (TPR) of 94% and a true negative rate (TNR) of 91.5% (TNR) corresponding respectively to the percentage of correctly classified samples in the “water leaks” and “normal lining” categories, respectively. Applied to a full-size image, the detection highlights the presence of water leaks, as shown in Figure 21.

Figure 21: Water leak detection (in blue) in images of a masonry tunnel

The second experiment aims at classifying the samples as “healthy” or “with defects”. These include surface defects typical of concrete tunnels: exposed reinforcement, pebble nests and wide cracks. The analysis of the results on a set of samples showed a TPR of 97.1% and a TNR of 95.9%. When we

applied this algorithm to the entire image, the detection of exposed reinforcements and pebble nests was visually correct. However, the algorithm seemed to have more difficulties to extract cracks (see Figure 22-left). Note that it was indeed possible to detect finer cracks, by using a specific training, but this is at the expense of a higher number of false alarms (Figure 22-right).

Figure 22: Defect detection (light areas) in concrete tunnel images. Example of a non-detected crack (blue box, left image). The same crack is detected using a more specific training (green box, right image) at the expense of a high rate of false alarms.

This exploratory work shows the relevance of supervised learning classification methods for automatically detecting defects in tunnels, despite the wide variability in the appearance of the linings and defects considered. The first results obtained on image samples give performances higher than 90% in terms of TPR and TNR. Quantifying performance on full-size image sequences, by comparison with a manually annotated base, should allow a finer analysis of the results. In perspective, we wish to explore other learning methods, such as deep learning, to increase detection performance. The use of convolutional neural networks (Goodfellow I. 2016) would also have the advantage of automatically learning the relevant descriptors.

6. CONCLUSION

In this paper, we have explored methods for reconstructing a whole tunnel. First, we reported on a first experiment in a lock, which highlighted the potentialities of a sonar for modelling a structure, and, in particular, its capacity to identify details. This experiment has shown that elements larger than 5 cm can be seen in the sonar model. In a second contribution, we have implemented and evaluated a 3D reconstruction pipeline of a canal tunnel from dynamic image and sonar acquisitions. Photogrammetry was used both to build the vault model and to compute the boat trajectory, which is necessary for georeferencing sonar data. An original approach has been proposed to build a reference model, based on laser and sonar static surveying. By computing distances between the dynamic model and the reference model, we provided quantitative results that showed a centimetric accuracy for photogrammetric reconstruction and a decimetric accuracy for underwater reconstruction.

Even if steps still need to be taken before a complete automation of the process can be achieved, this research has shown the feasibility of documenting engineering structures such as canal tunnels in 3D. The proposed techniques could also be generalized to areas where the GPS signal is inoperative. They are complementary to more classical bathymetry methods. Moreover, we have shown the feasibility of automatically detecting defects in the structure via pattern recognition methods, which may be generalized to other structures and to underwater elements.

In line with this collaborative research, and as part of its evolution towards digital technology, the so-called *VAF waterways* project, VNF is launching a first innovation partnership for high-throughput

collection of images of the linear components of its network (mainly embankments and dikes), from the waterway. The aim is to automatically pre-inform (using shape recognition technologies) the condition field in the VNF structure database. Moreover, the images will be made available through a geolocalized interface (similar to Google Riverview).

REFERENCES

Albert J.L., Charbonnier P., ChavantP. Foucher P., Muzet V., Prybyla D., Perrin T., Grussenmeyer P., Guillemin S., & Koehl, M. «Devising a visual inspection system for canal tunnels: preliminary studies.» *24th CIPA Symposium .* Strasbourg, France: ISPRS, 2013. 13-18.

Breiman L. «Random forests.» *Machine learning* (Springer) 45, n° 1 (2001): 5-32.

Charbonnier P., Foucher P., Chavant P., Muzet V., Prybyla D., Perrin T., Albert J.L., Grussenmeyer P., Guillemin S. & Koehl M. «An image-based inspection systme for canal-tunnel heritage.» *International Journal of Heritage in the Digital Era* 3, n° 1 (2014): 197-214.

Dalal N., & Triggs B. «Histograms of oriented gradients for human detection.» *Proceedings of International Conference on Computer Vsion and Pattern Recognition .* San diego, USA, 2005. 886-893.

Duvergier J. *5-6 août 1879, Loi relative au classement et à l'amélioration des voies navigables.* Vol. Tome soixante-dix-Neuvième, chez *Collection complète des lois, décrets, ordonnances, réglements et avis du conseil d'état*, de Noblet Ch., Larose L., 338-339. Bibliothèqe Nationale de France, Paris, 1879.

Fagon Y., Flaquet-Lacoux V., Brioist J.J., Dubois D. & Choquet C. «Tunnels canaux - fascicule 1 : surveillance, entretien, réparation.» Guide technique (in french), CETMEF, Compiègne, 2002.

Foucher P., Bah M.D., Charbonnier P. Boulogne C. & Larive C. «Classification automatique de défauts sur des images de tunnels par forêts d'arbres aléatoires.» *Congrès national sur la reconnaissnce de Formes et l'Intelligence Artificielle -(in french).* Clermont-Ferrand, France, 2016.

Golub G.H., Van Loan C.F. *Matrix computations.* 4th ed. John Hopkins, 2012.

Goodfellow I., Bengio Y. & Courville A. *Deep Learning.* MIT Press, 2016.

Haralick R., Shanmugam K. & Disntein I. «Textural features for image classification.» 3, n° 6 (nov 1973): 610-621.

Moisan E. «Imagerie 3D du "tube entier" des tunnels navigables.» Thèse de doctorat (in french), Université de Strasbourg, 2017.

Moisan E., Charbonnier P., Foucher P., Grussenmeyer P., Guillemin S. & Koehl M. «adjustment of sonar and laser acquisition for building the 3D refrence model of a canal tunnel.» *Sensors* 15, n° 2 (2015): 31180-21204.

Moisan E., Charbonnier P., Foucher P., Grussenmeyer P., Guillemin S., Samat O. & Pagès C. «Assessment of a static multibeam sonar scanner for 3D surveying in confined subaquatic Environments.» *International Archives of the photogrammetry remote sensing and spatial Information Sciences.* Prague, czech republic, 2016. 541-548.

Moisan E., Heinkele C., Charbonnier P., Foucher P., Grussenmeyer P., Guillemin S. & Koehl M. «Dynamic 3D modeling of a canal-tunnel using photogrammetric and bathymetric data.» *ISPRS Workshop "3D Arch".* Nafplio, Grèce, 2017. 495-501.

Rupnik E., Daakir M. & Pierrot Deseilligny M. «MicMac - a free open-source solution for photogrammetry.» *Open geospatial data, software and standards*, 2017.

Szeliski R. *Computer vision: algorithms and applications.* New York, USA: Springer-Verlag, 2010.

Tsai R.Y. «A versatile camera calibration technique for high-accuracy 3D machine-vision metrology using off-the-shelf TV cameras and lenses.» *IEEE Journal on Robotics and automation* 3, n° 4 (1987): 323-344.

Xiao Y., Wu J., & Yuan Y. «mCentrist: A multi-channel Feature Generation Mechanism for Scene Categorization.» *IEEE transactions on Image processing* 23, n° 2 (2014): 823-836.

Zhang Z. «flexible camera calibration by viewing a plane from unknown orientations.» *Proceedings of the seventh IEEE International conference on computer vision (ICCV).* Kerkyra, Corfou, Grèce: IEEE, 1999. 666-673.